atmosphere

MDPI

Article

Evaluation of Eutrophication in Jiaozhou Bay via Water Color Parameters Determination with UAV-Borne Hyperspectral Imagery

Xin Pan [1,2], Zhangjun Wang [1,3,*], Habib Ullah [4], Chao Chen [1,3], Xiufen Wang [1], Xianxin Li [1,3], Hui Li [1], Quanfeng Zhuang [1], Boyang Xue [1,3] and Yang Yu [1]

[1] Institute of Oceanographic Instrumentation, Qilu University of Technology (Shandong Academy of Sciences), Qingdao 266001, China
[2] College of Environment and Safety Engineering, Qingdao University of Science and Technology, Qingdao 266042, China
[3] R & D Center for Marine Instruments and Apparatuses, Pilot National Laboratory for Marine Science and Technology (Qingdao), Qingdao 266200, China
[4] Department of Environmental Science, Zhejiang University, Hangzhou 310058, China
* Correspondence: zhangjunwang@qlu.edu.cn

Abstract: The continued increase in greenhouse gas emissions as a result of unprecedented eutrophication has resulted in a rising trend of red tides in the sea, which may be responsible for ecological degradation in the surrounding environment. Studies rarely investigate the accurate concentration of seawater eutrophication substances in offshore aquaculture areas, which may lead to the exacerbated pollution of inshore aquaculture. We examined whether offshore seawater quality monitoring can be effectively performed through unmanned aerial vehicles' (UAVs) airborne hyperspectral remote sensing technique at Jiaozhou Bay, a water body associated with eutrophication. We used the UAV airborne hyperspectral imager to detect and measure typical marine aquaculture areas in Jiaozhou Bay and selected the key parameters of seawater quality, chlorophyll-a (Chl-a) concentrations, and total suspended matter (TSM) concentrations as indicators of seawater eutrophication. The hyperspectral inversion model of the Jiaozhou Bay seawater (JZBZ) was established with the optimal sensitive band of parameters. Results showed that in comparison with the traditional inversion model, the inversion R^2 of the Chl-a was 0.712, the RPD was 3.72, and the inversion R^2 of the TSM concentration was 0.756 while the RPD was 5.83. We found that this model is more suitable for the retrieval of water color parameters in Jiaozhou Bay. Additionally, by actual measurement, it can be seen that the concentration ranges of Chl-a in the observation area are 0.380–1.74 mg/m^3, and the concentration range of TSM is 12.6–131 mg/L. The results of this study indicate that the Jiaozhou Bay Water Quality Translation Model (JZBM), based on the UAV airborne hyperspectral imager, performs well in the inversion of the concentration of chlorophyll and suspended particulate matter in offshore water, which advances our understanding with a new method to assess the degree of eutrophication in coastal waters.

Keywords: chlorophyll-a; hyperspectral inversion model; total suspended matter; optical properties

Citation: Pan, X.; Wang, Z.; Ullah, H.; Chen, C.; Wang, X.; Li, X.; Li, H.; Zhuang, Q.; Xue, B.; Yu, Y. Evaluation of Eutrophication in Jiaozhou Bay via Water Color Parameters Determination with UAV-Borne Hyperspectral Imagery. *Atmosphere* **2023**, *14*, 387. https://doi.org/10.3390/atmos14020387

Academic Editors: Peng Zhang, Chuancheng Fu and Jian Liu

Received: 30 January 2023
Revised: 9 February 2023
Accepted: 12 February 2023
Published: 16 February 2023

1. Introduction

Owing to the progressive land use changes, deforestation, and combustion of fossil fuels, the emission of greenhouse gases has dramatically increased, which has resulted in marine eutrophication, flooding, and other serious global challenges [1]. In recent years, mariculture has become a rapidly expanding global market due to rising seafood consumption, which is anticipated to reach 102 million metric tons by 2025 in order to meet the increasing demand for high-quality protein [2]. Due to continued demand growth, China is seeing massive development in the aquaculture sector, providing more than 60% of global aquaculture production [3].

The Sustainable Development Goals (SDGs) state that one of the biggest issues confronting human societies worldwide is how to sustainably satisfy the requirements of 9.7 billion individuals for food and livelihoods in 2030 [4] while contending with the effects of climate change and environmental degradation [5]. Aquaculture, which is growing at the quickest rate among the main food manufacturing industries, is increasingly seen as a promising way to address population expansion by supplying food and nutrition, providing jobs and means of subsistence, and generating income through the sale of fish and seafood [6]. From 2000 to 2018, the percentage of fish produced through aquaculture increased from 27% to 46% [7].

Despite offshore freshwater aquaculture being a little more prevalent, its growth is restricted by a lack of land and freshwater availability [8]. In contrast, there are no such restrictions on global marine and coastal aquaculture, an area that has been expanding quickly over the past 20 years. The total yield increased from 14.2 million tons in 2000 to 30.8 million tons in 2018, accounting for 38% of the total global aquaculture yield in 2018 [9]. Since 1991, China has produced more aquaculture food than the rest of the world combined, and since 2002, it has surpassed all other countries as the world's top exporter of fish and fish products (FAO, 2018). China alone produced 64.6 million tons of aquatic products in 2018, of which aquaculture accounted for 77% [7].

In the meantime, land acquisition led to the intensive utilization of the natural shoreline, which resulted in a decrease in sea area, hydrodynamic force, and tidal prism in the bays [10]. These modifications led to inadequate seawater circulation and significantly reduced the ability for sewage to spread. Red tide catastrophes have been occurring frequently in the bays as a result of eutrophication brought on by declining water quality [11]. This has put a tremendous amount of pressure on aquatic environments and threatened the sustainable development of the economy and society in coastal regions [12].

Unreasonable aquaculture practices, excessive aquaculture production, and a large amount of pollution discharged directly into marine aquaculture will cause red tides, enteromorpha, and other disasters. These issues lead to serious environmental pollution, ecological imbalance, and eutrophication of coastal waters. In order to reduce pollution discharge at the source and stop the degradation of mariculture water quality, it is necessary to quickly and accurately understand the temporal and spatial characteristics, evolution process, influencing factors, and other information of mariculture water quality parameter concentrations [13].

Remote sensing [14] is the process of deriving valuable information regarding surfaces from data collected by a sensor, also known as a spectrometer or spectroradiometer, that is either integrated on a satellite, plane, or unmanned aerial vehicle (UAV) for imaging spectroscopy, handled by an operator, or remedied on a launch pad for field spectroscopy. This technology's ability to survey enormous regions in an unobtrusive and non-damaging manner is one of its key benefits. Multispectral imaging spectrometers use the sun as their radiation source to detect the reflectance of surfaces, or the reflected solar radiation, spanning a few broad spectral bands of the optical domain [15]. Unmanned aerial vehicle remote sensing technology has evolved as a result of the modern technology boom and the rising demand for remote sensing imagery. UAV remote sensing technology has advanced rapidly over the past decade and is extensively employed in a variety of industries, including disaster and emergency management, agriculture surveillance, mapping and surveying, and national defense. The necessity for efficient and timely monitoring is currently growing as a result of marine biological and environmental issues that are becoming more significant. Compared with traditional marine monitoring technology, UAV remote sensing has become a new marine monitoring method because of its adaptability and effectiveness. It also produces statistical information with high spatial and temporal resolutions [16].

Aquaculture water quality metrics are complicated, and marine aquaculture pollution is a non-point source of pollution. Conventional laboratory water quality monitoring techniques suffer from inadequate timeliness, discontinuity, and limited scope due to the features of multi-variability, nonlinearity, and fluidity [17]. Additionally, it is challeng-

ing to implement large-scale and dynamic monitoring techniques. With the continued advancement of remote sensing technology, hyperspectral remote sensing technology has become widely used in remote sensing water quality monitoring, greatly increasing the estimation accuracy of remote sensing monitoring water quality parameters [18]. Hyperspectral remote sensing technology has the advantages of high precision, multi-band, and large amounts of information [19]. The concentrations of Chl-a, TSM, and colored soluble organic matter are several important indicators for evaluating the impact of aquaculture water on the ecological environment. They can reveal and characterize the existing amount of phytoplankton in the sea area, as well as reflect seawater eutrophication. The crucial step in assessing the pollution caused by marine aquaculture is to establish an inversion model [20].

Vahtmae et al. [21] used hyperspectral remote sensing to measure the growth of benthic macroalgae in coastal waters under eutrophic conditions and verified the feasibility of hyperspectral remote sensing for monitoring eutrophic waters. Moreover, Hunter et al. [22] used hyperspectral remote sensing of cyanobacterial pigments as indicators of cell populations and toxins in eutrophic lakes. Song et al. [23] used genetic algorithm-partial least squares (GA-PLS) modeling and performed hyperspectral determination of eutrophication in water bodies. However, it is difficult for the above spaceborne hyperspectral technologies to achieve high spatial resolutions of images at the same time, which restricts the acquisition of information in the spatial dimension. Airborne hyperspectral remote sensing has the advantages of high spatial resolution, high temporal resolution, and flexible image acquisition, which provides a new way for the application of regional water quality monitoring [16]. Bansod et al. carried out a spectral evaluation of chlorophyll-a, turbidity, and total phosphorus concentration in the Ganges River with an airborne visible/infrared imaging spectrometer. Using airborne hyperspectral images, Niu et al. [24] used deep learning to accurately measure optically active parameters, such as chlorophyll-a (Chl-a), cyanobacteria, and colored dissolved organic matter (CDOM).

The vast majority of related studies employed aerial hyperspectral technology to track changes in water quality in pristine water bodies, such as deep seas, inland lakes, reservoirs, and rivers. Although there has been some research on remote sensing monitoring and pollution assessment of offshore mariculture water quality, it is still important to further investigate the most appropriate theories and techniques. As a result, Jiaozhou Bay's typical marine aquaculture area was chosen as the research area for this paper, which considers the use of airborne hyperspectral technology. The essential metrics of seawater quality selected as monitoring indicators were the chlorophyll-a concentration and suspended sediment mass concentration. Aquaculture data were obtained using field measurements. The characteristics of the changes in the aquaculture water quality parameters and their influencing factors were analyzed based on the hyperspectral data and water quality monitoring data of the nearby water body. Additionally, the correlation between the concentration of each parameter and the spectral reflectance was analyzed. High-quality aquaculture water quality was established based on the most sensitive band of water quality parameters. The spectral inversion model was used to invert the concentration of water quality parameters in aquaculture areas to analyze spatio-temporal characteristics. To our knowledge, only limited attempts have been made to investigate the eutrophication in Jiaozhou Bay using water color parameter determination with UAV-borne hyperspectral imagery. This study provides a reference for remote sensing monitoring of water quality in mariculture.

2. Materials and Methods

2.1. Study Area

The study area in this paper was chosen as Jiaozhou Bay, located in the northern part of China (35.97°–36.30° N, 120.07°–120.38° E), as shown in Figure 1. Jiaozhou Bay is located in a warm temperate zone with relatively low temperatures (12.2 °C on average per year) and 776 millimeters of annual rainfall. With more than 10 rivers draining into Jiaozhou

Bay, it has a significant drainage area of 7800 km^2 [25]. Jiaozhou Bay, located south of Shandong Peninsula, is a typical temperate semi-enclosed shallow bay with an average depth of approximately seven meters and a surface area of around 374 km^2 that connects to the northwest of the South Yellow Sea [2]. Its coast has experienced residential and industrial pollution in recent years. The eastern coast of Jiaozhou Bay, where Qingdao City's major ports and industries are located, is heavily impacted by human activity. The Loushan River, Licun River, and Haipo River, in particular, have evolved into the primary entry points for domestic and industrial sewage into the bay [26]. Aquaculture is the main economic pillar of the coastal area, and a large amount of aquaculture wastewater is directly discharged into Jiaozhou Bay, resulting in an upward trend in the concentration of nutrients in Jiaozhou Bay.

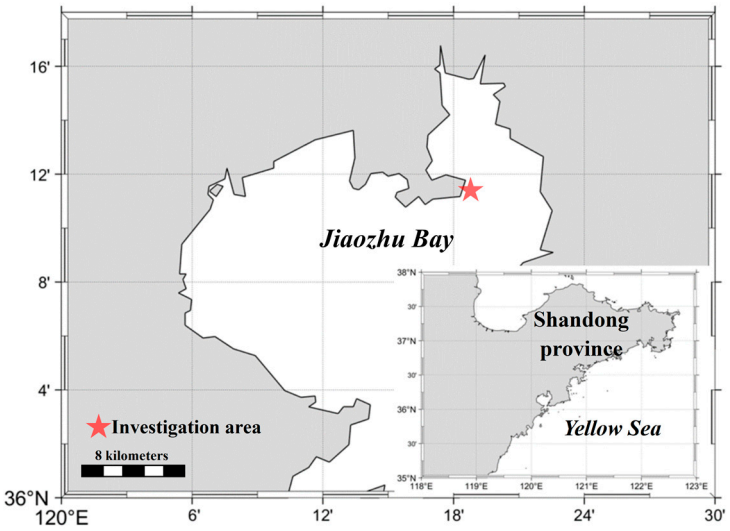

Figure 1. Map of the study area.

The red box in Figure 1 represents the current research area. Numerous fishing boats and fishermen can frequently be seen working in the area, where there are many breeding sites for aquatic organisms, such as sea cucumbers and bamboo shrimp. There are also reports that the pollution from breeding wastewater in Jiaozhou Bay has seriously degraded the quality of the seawater and poses a high environmental risk to nearby aquatic organisms. In general, Jiaozhou Bay's water quality has an impact on both the social economy's sustainability and the health of the local populace.

2.2. Data Acquisition

2.2.1. Observation of UAV Images

The marine surface was observed by the push-broom airborne ocean hyperspectral imager Pika L (Resonon, Inc., Bozeman, MT, USA) and it's parameters were listed in Table 1. DJI M600Pro UAV (M600 PRO UAV DJI, Co., Ltd., Shenzhen, China) was used for a flight test. Precise spectral calibrations and radiometric calibrations were performed using a monochromator and an integrating sphere. The hyperspectral image was collected on 20 November 2021. According to the frame rate and field of view of the airborne hyperspectral instrument design, the flight altitude was 150 m and the flight speed was 2.5 m/s, so the ground spatial resolution of the image pixel was 0.05 m. In order to ensure the overlap of images on adjacent routes, the distance between adjacent routes was 40 m. In order to collect and process spectral data under certain environmental conditions, such as a clear sky with small cloud cover or full cloud coverage, a generally calm water surface, uniform light conditions, sea state level 3 and below, and moderate wind and waves, the flight trajectory design as shown in Figure 2 was chosen.

Table 1. Hyperspectral imager parameters.

Index	Performance
Detection wavelength range	400 nm~1000 nm
Spectral resolution	>2.5 nm
Angular resolution	>0.6 mrad
Maximum sampling frequency	≥200 Hz

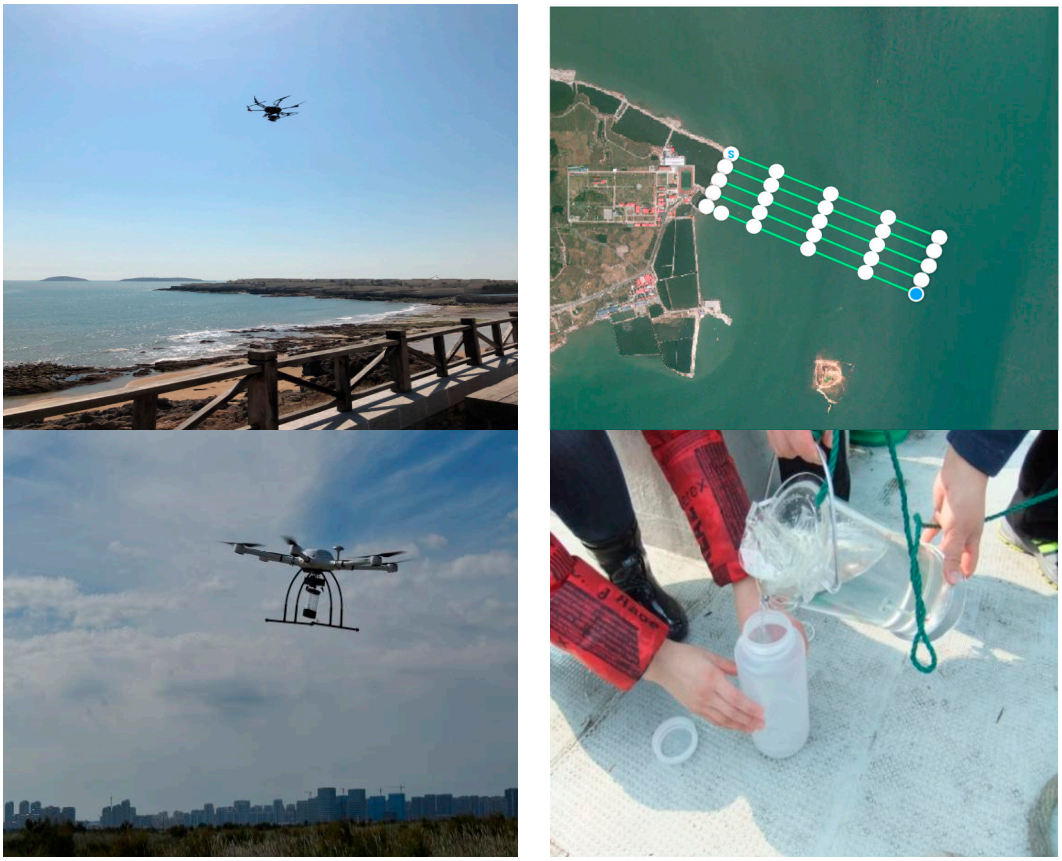

Figure 2. Operation map, route planning, and water sample collection diagram.

2.2.2. Field Data Collection

The sampling points for the present study are shown in Figure 2. The temperature of the study area was 1–3 °C, the humidity was 73%, and it was cloudless with ample light. During the collection of the hyperspectral data, the passing sediments were readily stirred up once the ship approached since the study site was near the coast and the water was shallow. As a result, when we arrived at the designated sampling locations, we had to wait for a while. The water sample collector outfitted with the UAV collected a total of 30 water samples from the seawater surface, as depicted in Figure 2. The water quality analysis was performed in the lab after the water samples were frozen and preserved. The concentrations of Chl-a and suspended solids in the collected seawater samples were determined by spectrophotometry (GBT 12763.6-2007; GB 17378.7-2007) and the gravimetric method (GB 17378.4-2007), respectively.

The NASA bio-optics specification (NASA/TM-2003-211621/Rev4-Vol.IV) is used to determine the absorption coefficient of yellow compounds. In order to filter water samples with a capacity of 2000 mL for Chl-a, Whatman GF/F glass microfibre filters (0.7 m pore size) were employed. Acetone with a volume fraction of 90% was then applied in order to extract the pigments. Using a Cary 5000 UV-Vis-NIR spectrophotometer, the level of Chl-a was measured. Water samples with a 1000-mL capacity were filtered for

TSM using Whatman cellulose acetate filters with a 0.45-m pore size. The filters were then gravimetrically weighted to calculate the TSM content. To prevent the entrance of external impurities while testing in the lab, the test equipment was thoroughly sterilized and dried just before a new sample was measured, as well as throughout the measurement procedure.

2.3. Data Processing Flow

2.3.1. Spectral Pre-Processing

Radiation calibration, atmospheric correction, picture filtering, geometric correction, and flight belt mosaicking are all included in image pre-processing. The radiometric calibration of the hyperspectral images converted the digital number to radiance. Images were atmospherically corrected after radiometric calibration to remove atmospheric and light effects. In order to obtain a more realistic spectrum, preprocessing work (such as removing abnormal spectra affected by solar flares and shadows, correcting dark noise, averaging multiple acquired spectra, etc.) was carried out. After that, remote sensing reflectance (Rrs) was calculated according to the formula.

$$R_{rs} = \frac{\gamma \cdot \left(L_{sw} - \tau \cdot L_{sky}\right)}{\pi \cdot L_p} \tag{1}$$

where L_{sw}, L_{sky}, and L_p were the upwelling radiance from water, the radiance of the skylight, and the reference panel, respectively. γ is the irradiance reflectance of the reference panel, and τ is a proportionality coefficient that relates Lsky to the reflected sky radiance determined when the detector viewed the water surface.

The Pearson correlation coefficient (ranging from -1 to 1) was used to characterize the correlation between each spectral band and chlorophyll concentration, and the larger the value, the stronger the correlation. The specific formula is as follows:

$$R = \frac{\sum_{i=1}^{n} (x_i - \overline{x})(y_i - \overline{y})}{\sqrt{\sum_{i=1}^{n} (x_i - \overline{x})^2 \sum_{i=1}^{n} (y_i - \overline{y})^2}} \tag{2}$$

where n is the sample size, x_i and y_i are the individual sample points of i, and x and y are the mean values of the samples.

2.3.2. Model Validation

The model accuracy of the water quality parameters was assessed by the determination coefficient (R^2), RMSE, relative RMSE (rRMSE), mean absolute errors (MAE), and prediction deviation ratio (RPD):

$$R^2 = \frac{\sum_{i=1}^{n} (x_i - \overline{y})^2}{\sum_{i=1}^{n} (y_i - \overline{y})^2} \tag{3}$$

$$RMSE = \sqrt{\sum_{i=1}^{n} (x_i - y_i)^2 / N} \tag{4}$$

$$MAE = \frac{\sum_{i=1}^{n} |x_i - y_i|}{n} \tag{5}$$

$$PRD = \sqrt{\frac{\sum x^2 - (x^2/n)/(n-1)}{\sum (x-y)^2 - \left[(x-y)^2/n\right]/(n-1)}} \tag{6}$$

where x_i or y_i are predicted or measured Chl-a and TSM concentration values, and n is the sample size.

3. Results and Discussion

3.1. Data Processing

Although Jiaozhou Bay's water quality is pure and the seawater spectrum for this study was gathered in winter, other external elements such as light and wind direction may also have an effect on the data collection, making the water body's spectral features in this region more complex. The spectral curves of 31 collection points were obtained from the preprocessed image according to the GPS coordinates of the seawater sample collection points, and the water body remote sensing reflectance curve was obtained after Savitzky-Golay filtering to smooth and remove noise, as shown in Figure 3. As seen in Figure 3, filtering has a very consistent trend on the spectral curve in the 400–900 nm region, and the interference signals are mostly eliminated. The spectral features of the nearshore water bodies in the Jiaozhou Bay sea region largely correspond to the features of the second-class water bodies, but they have their own distinctiveness, as can be observed from the trend of the spectral curves of the water bodies at each sampling site. The remote sensing reflectance of sea surface water varies with wavelength. The remote sensing reflectance value in the range of 400–500 nm is low, which may be caused by the strong absorption of colored soluble organic matter and Chl-a. In particular, there is a reflection trough between 420 and 440 nm, which is caused by the absorption of blue-violet light by Chl-a in the algae. With an increase in Chl-a concentration, the reflection peak, which is typically thought of as the fluorescence peak of Chl-a, reappears in the 670–700 nm range. Its position and reflectance move in the direction of long waves. The reflection peak is an additional peak in the spectrum of suspended sediment reflectance. The reflection peak will shift to the long-wave direction as the amount of suspended sediment in the water rises, causing a red shift phenomenon [27].

According to the different optical properties of water bodies, water bodies are usually divided into Type I water bodies and Type II water bodies (Class I and Class II) [28]. The optical characteristics of Class I water bodies are mainly affected by phytoplankton and their companions (the debris produced during decomposition) in the water body. This debris is related to phytoplankton. Open ocean waters are typical Class I water bodies. Its area accounts for more than 90% of the global ocean area. At present, the error of commercialized chlorophyll-a concentration products in Type I water bodies is about 30–35% [29]. The composition and optical properties of Type II water bodies are usually more complex than those of Type I water bodies, and their optical properties are not only affected by phytoplankton and their companions but also by inorganic suspended matter and colored soluble organic matter in the water body [30]. There is no correlation between properties and phytoplankton, so the interpretation of the optical signal in Type II water is more difficult. Generally, Class II water bodies are mainly located in places near shores and estuaries that are seriously affected by the discharge of terrestrial substances. These are the sea areas that are closest to humans and suffer the greatest impact from human activity [31]. Therefore, water color remote sensing of Class II water bodies has become difficult and a hotspot in water color remote sensing technology. Water color remote sensing data are primarily centered on Type I water bodies because they are very simple and clear, and there are operational methods that are well validated; however, the current standard algorithm for retrieving chlorophyll is not suited for Type II water bodies. The sea area of Jiaozhou Bay is a semi-enclosed bay and a Class II water body. By combining the measured spectral data and the water body component concentration data synchronously measured by the laboratory, an empirical inversion algorithm for each water color element was established to improve the performance of the hyperspectral equipment. Additionally, online analysis and processing software optimization were crucial.

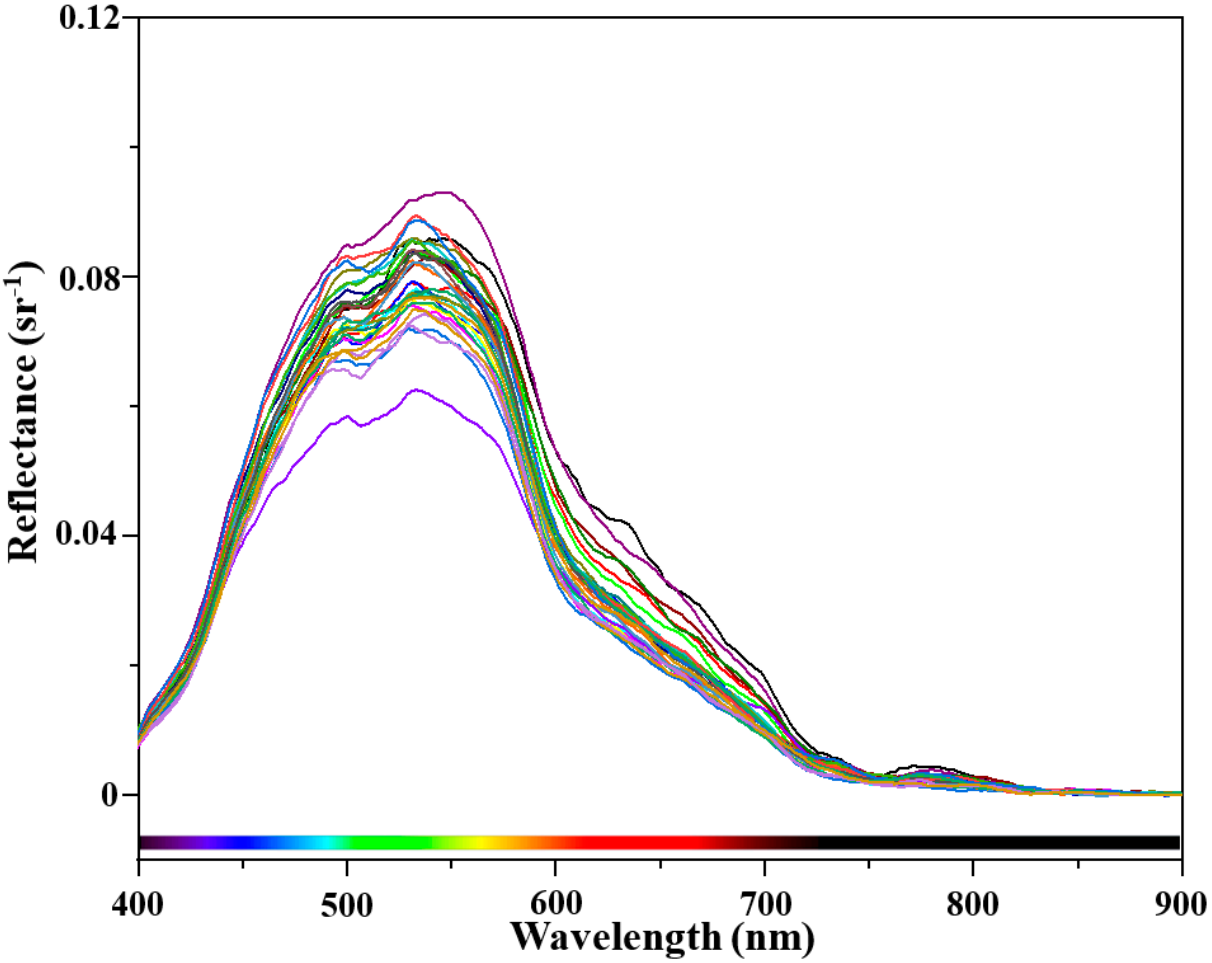

Figure 3. Water spectral curves of the seawater sampling sites.

Currently, the Chl-a concentration inversion algorithm employed in water color remote sensing is primarily an empirical algorithm. A single or multiple regression relationship suitable for a particular environment can be found by using the regression method to establish the remote sensing reflectance ratio or value itself and the concentration of a particular water body component in different bands (such as the relationship between the concentration of chlorophyll-a). Among them, many studies have shown that the NSOAS model proposed by Tang on the basis of the Tassan model is suitable for the Chinese sea area, and the inversion model of the concentration of Chl-a and TSM is shown in the equations below:

$$lgC = a_0 + a_1 lgx_1 + a_2 lg^2 x_1 \quad (7)$$

$$lgS = b_0 + b_1 x_2 + b_2 x_3 \quad (8)$$

$$x_1 = \left(R_{rs(443)}/R_{rs(555)}\right)\left(R_{rs(412)}/R_{rs(490)}\right) \quad (9)$$

$$x_2 = R_{rs(555)} + R_{rs(670)} \quad (10)$$

$$x_3 = R_{rs(490)}/R_{rs(555)} \quad (11)$$

where a_0–a_2 and b_0–b_2 were fitting coefficients. The sensitivity of each band to chlorophyll and suspended particles was investigated using measured spectrum data from the testing station in the Jiaozhou Bay sea region and the measured suspended solids content of the corresponding seawater samples. Figure 4 demonstrates that 31 sampling points were used. The bands of 421, 447, 533, and 624 nm were clearly more associated with the concentration of Chl-a. Similarly, there was a significantly stronger correlation between

the TSM concentration and the 502, 570, and 660 nm bands. On the basis of NSOAS, a new water color retrieval model suitable for Jiaozhou Bay was developed, taking into account the form of a single-band polynomial and a multi-band ratio logarithmic sum:

$$lg(Chla) = c_0 + c_1 lg x_4 + c_2 lg^2 x_4 + c_3 lg^3 x_4 + c_4 lg^4 x_4 \quad (12)$$

$$lg(TSM) = d_0 + d_1 x_5 + d_2 x_6 + d_3 x_5 x_6 + d_4 x_5 / x_6 \quad (13)$$

$$x_4 = \left(R_{rs(447)} / R_{rs(624)}\right)\left(R_{rs(421)} / R_{rs(533)}\right) \quad (14)$$

$$x_5 = R_{rs(570)} + R_{rs(660)} \quad (15)$$

$$x_6 = R_{rs(502)} / R_{rs(570)} \quad (16)$$

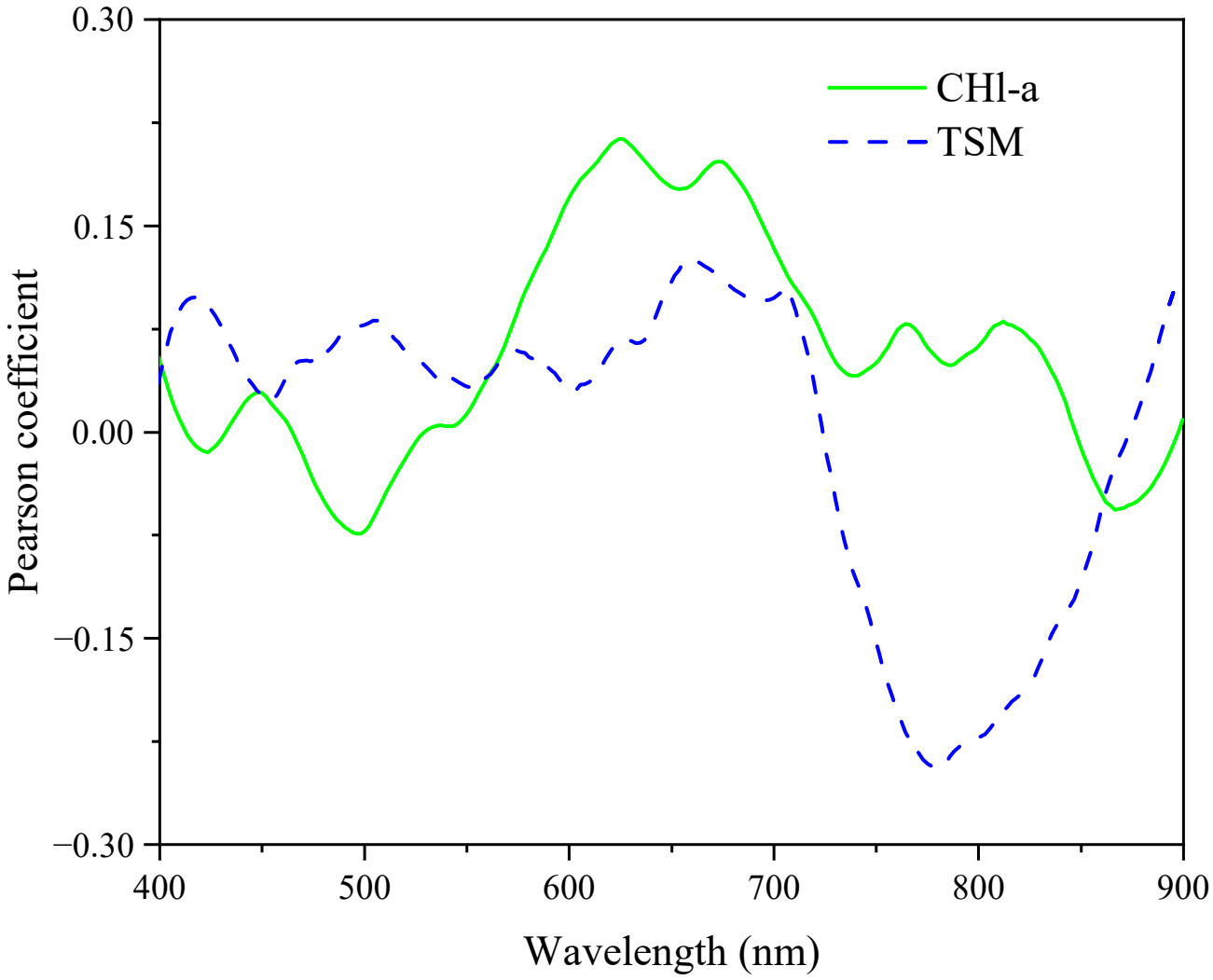

Figure 4. Correlation between normalized spectra Chl-a and TSM.

3.2. Observation Chart and Laboratory Comparison Chart

Subsubsection

Figure 5 compares the estimated and measured values of Chl-a and TSM for 31 seawater sample collection sites. It compares the two models, JZBM and NSOAS, showing that for measured TSM, R^2 grew from less than 0.39 to 0.71 (Figure 5a), whereas for Chl-a, R^2 increased from 0.39 to 0.71. (Figure 5b). It can also be used to describe the accuracy analyses of several models, including JZBM and NSOAS. It is possible to argue that the novel model JZBM was superior to the NSOAS model for retrieving the Chl-a con-

centration in the research region and that its RMSE and MAE were lower for both measured TSM and Chl-a. It has been demonstrated that the proposed model, when used to retrieve Chl-a concentration in Qingdao's coastal waters, has higher accuracy and more benefits.

The R^2 of the improved JZBM model reached 0.71, the RPD was 3.72, and the fitting accuracy of the model was greatly improved. It can be inferred that the JZBM model is more suitable for the inversion of the studied parameters in Jiaozhou Bay and can better assess the extent of seawater eutrophication in the Jiaozhou Bay aquaculture area.

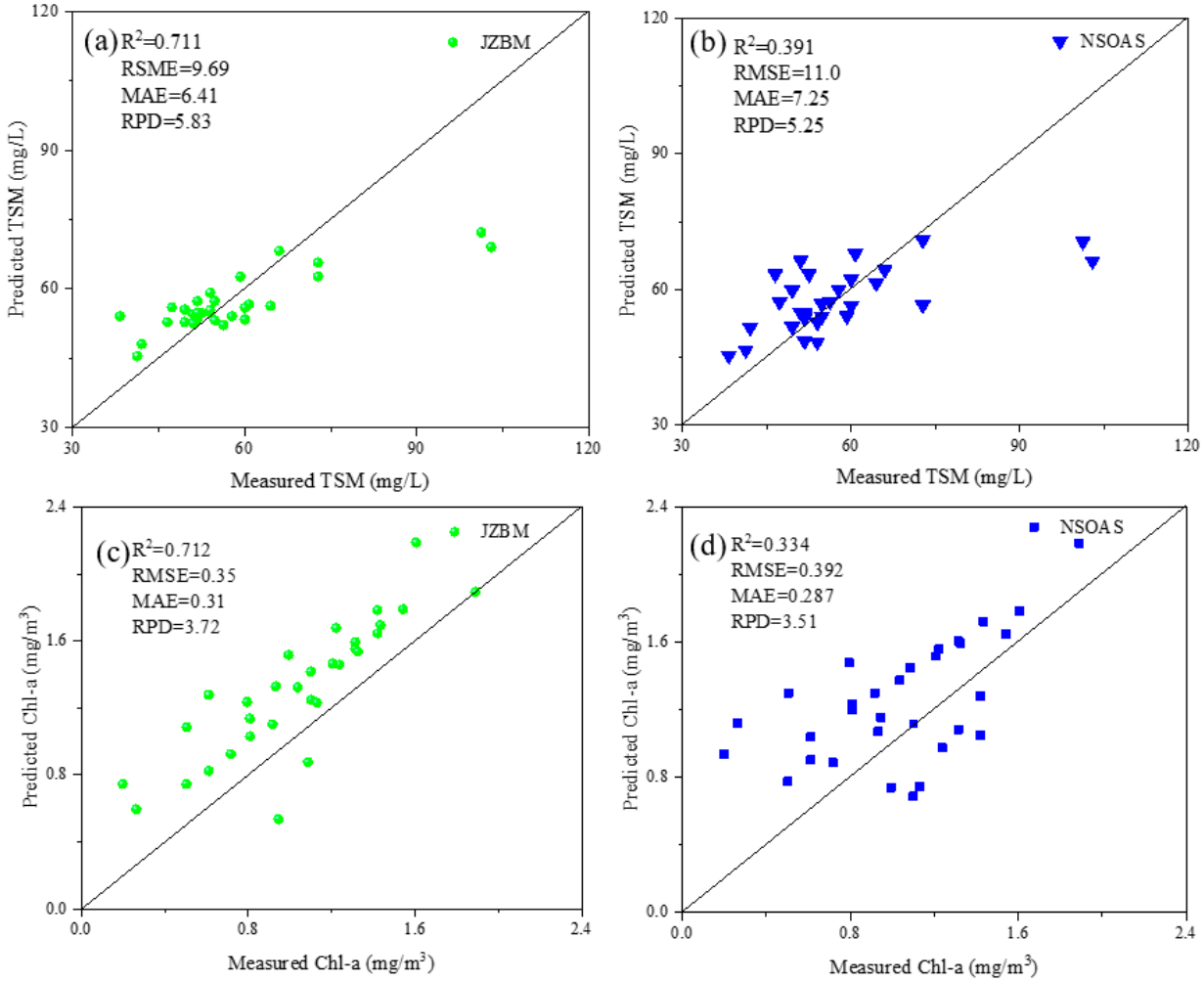

Figure 5. Comparison of the estimated and measured values of the TSM concentration by JZBN model (**a**) and NSOAS model (**b**), and the Chl-a concentration by JZBN model (**c**) and NSOAS model (**d**).

3.3. Spatial Distribution of Chl-a and TSM

The spatial distributions of the Chl-a and TSM concentrations in the study area were estimated and depicted in Figure 6 in accordance with the established JZBM inversion model of Chl-a and TSM concentrations, which was applied to the hyperspectral data acquired by the aerial hyperspectrometer. Chl-a concentrations ranged from 0.38 to 1.74 mg/m^3, as depicted in Figure 6. The concentration of Chl-a on the shore was slightly lower than in the open sea due to the limited size of the study region, which made it difficult to discern the general changing trend of Chl-a. Additionally, there was a very evident pattern of change as the concentration of TSM varied between 12.6 and 131 mg/L and was higher at the coast than in the open sea.

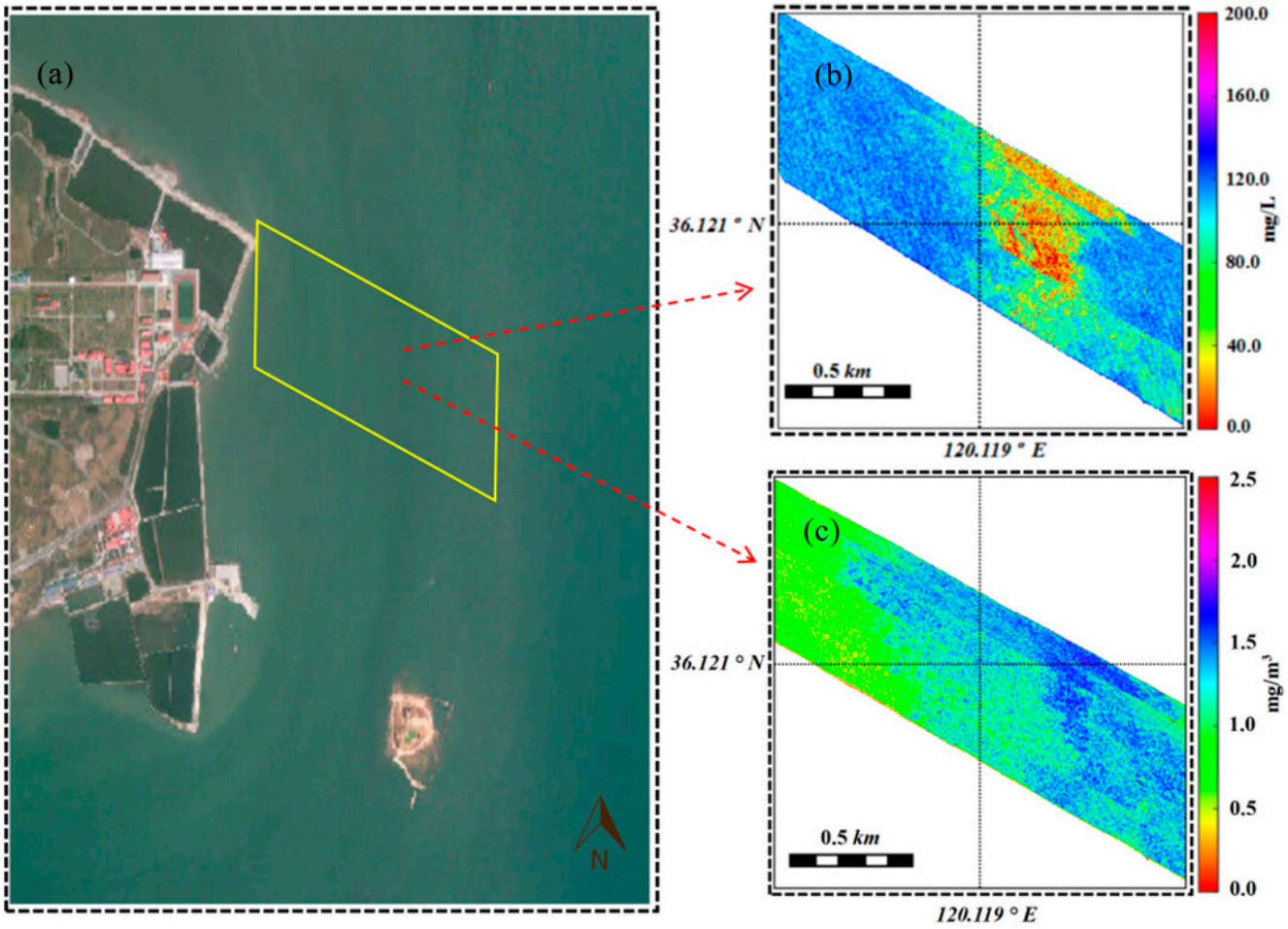

Figure 6. The study area (**a**) spatial distributions of the TSM (**b**) and Chl-a (**c**) concentrations in.

4. Conclusions

This study demonstrates the feasibility of UAV airborne hyperspectral remote sensing technology as a rapid assessment tool to determine the concentration and spatial distribution of water quality parameters in the Jiaozhou Bay sea area. According to the study results, hyperspectral images are a good tool for tracking Jiaozhou Bay water quality characteristics. According to the relationship between the spectral characteristics of the hyperspectral image of the water body and the sensitivity of the characteristic band, a JZBM water quality inversion model for Jiaozhou Bay was established. The JZBM model has high prediction accuracy for the two water quality parameters, Chl-a and TSM, and the Rp2 values are both greater than 0.7. Through the analysis of indoor test data and field investigations of the research area, the spatial distribution map of Chl-a concentrations and TSM concentrations in the Jiaozhou Bay area was obtained, which accurately reflects the current situation and has high regional value. Overall, this study will provide a powerful tool to quickly assess the degree of eutrophication in Jiaozhou Bay.

Author Contributions: Conceptualization, X.P.; methodology, Z.W. and C.C.; validation, B.X.; formal analysis, Q.Z.; resources, H.L., Q.Z. and X.L.; data curation, Z.W. and Y.Y.; writing—original draft preparation, Q.Z.; writing—review and editing, Z.W., X.P., X.W. and H.U.; visualization, H.L. and X.P.; supervision, Z.W.; project administration, C.C., X.W. and Y.Y., funding acquisition, B.X. All authors have read and agreed to the published version of the manuscript.

Funding: This paper is supported by the National key Research and Development Program (2022YFC2807202, 2021YFB3901304), Shandong key Research and Development Program (2020CXGC010104, 2022CXPT020), Qingdao Pilot National Laboratory for Marine Science and Technology (2021WHZZB0205), Qingdao key technology project (22-3-3-hygg-13-hy), Development Fund Project of IOISAS (HYPY202106).

Data Availability Statement: Data are not publicly available, though the data may be made available on request from the corresponding author.

Conflicts of Interest: The authors declare that the research was conducted in the absence of any commercial or financial relationships that could be construed as a potential conflict of interest.

References

1. Hong, C.; Burney, J.A.; Pongratz, J.; Nabel, J.E.; Mueller, N.D.; Jackson, R.B.; Davis, S.J.J.N. Global and regional drivers of land-use emissions in 1961–2017. *Nature* **2021**, *589*, 554–561. [CrossRef] [PubMed]
2. Liu, F.-F.; Zhang, Y.-X.; Lu, T. Performance and mechanism of constructed wetland-microbial fuel cell systems in treating mariculture wastewater contaminated with antibiotics. *Process Saf. Environ. Prot.* **2023**, *169*, 293–303. [CrossRef]
3. Chen, F.; Lao, Q.; Liu, M.; Huang, P.; Chen, B.; Zhou, X.; Chen, P.; Chen, K.; Song, Z.; Cai, M. Impact of intensive mariculture activities on microplastic pollution in a typical semi-enclosed bay: Zhanjiang Bay. *Mar. Pollut. Bull.* **2022**, *176*, 113402. [CrossRef] [PubMed]
4. Calicioglu, O.; Flammini, A.; Bracco, S.; Bellù, L.; Sims, R. The future challenges of food and agriculture: An integrated analysis of trends and solutions. *Sustainability* **2019**, *11*, 222. [CrossRef]
5. Wijerathna-Yapa, A.; Pathirana, R. Sustainable Agro-Food Systems for Addressing Climate Change and Food Security. *Agriculture* **2022**, *12*, 1554. [CrossRef]
6. Taylor, S.F.; Roberts, M.J.; Milligan, B.; Ncwadi, R. Measurement and implications of marine food security in the Western Indian Ocean: An impending crisis? *Food Secur.* **2019**, *11*, 1395–1415. [CrossRef]
7. Wu, J.; Del Valle, T.M.; Ruckelshaus, M.; He, G.; Fu, Y.; Deng, J.; Liu, J.; Yang, W. Dramatic mariculture expansion and associated driving factors in Southeastern China. *Landsc. Urban Plan.* **2021**, *214*, 104190. [CrossRef]
8. Holmer, M. Environmental issues of fish farming in offshore waters: Perspectives, concerns and research needs. *Aquac. Environ. Interact.* **2010**, *1*, 57–70. [CrossRef]
9. Lim, H.R.; Khoo, K.S.; Chew, K.W.; Chang, C.-K.; Munawaroh, H.S.H.; Kumar, P.S.; Huy, N.D.; Show, P.L. Perspective of Spirulina culture with wastewater into a sustainable circular bioeconomy. *Environ. Pollut.* **2021**, *284*, 117492. [CrossRef]
10. Huang, Y.; Li, Z.; Sun, C.; Feng, Z.; Li, J.; Wei, D.; Wang, B.; Jiang, S.; Chen, K.; Sun, X. Using the roughness height and manning number in hydrodynamic model to estimate the impact of intensive oyster aquaculture by floating & fixed rafts on water exchange with an application in Qinzhou bay, China. *Ecol. Model.* **2023**, *476*, 110230. [CrossRef]
11. Zhang, H.-X.; Shen, Y.-M.; Tang, J. Numerical investigation of successive land reclamation effects on hydrodynamics and water quality in Bohai Bay. *Ocean Eng.* **2023**, *268*, 113483. [CrossRef]
12. Leka, A.; Lagarias, A.; Panagiotopoulou, M.; Stratigea, A. Development of a Tourism Carrying Capacity Index (TCCI) for sustainable management of coastal areas in Mediterranean islands–Case study Naxos, Greece. *Ocean Coast. Manag.* **2022**, *216*, 105978. [CrossRef]
13. Zhang, X.; Zhang, Y.; Zhang, Q.; Liu, P.; Guo, R.; Jin, S.; Liu, J.; Chen, L.; Ma, Z.; Liu, Y. Evaluation and analysis of water quality of marine aquaculture area. *Int. J. Environ. Res. Public Health* **2020**, *17*, 1446. [CrossRef] [PubMed]
14. Aasen, H.; Honkavaara, E.; Lucieer, A.; Zarco-Tejada, P. Quantitative remote sensing at ultra-high resolution with UAV spectroscopy: A review of sensor technology, measurement procedures, and data correction workflows. *Remote Sens.* **2018**, *10*, 1091. [CrossRef]
15. Lassalle, G. Monitoring natural and anthropogenic plant stressors by hyperspectral remote sensing: Recommendations and guidelines based on a meta-review. *Sci. Total Environ.* **2021**, *788*, 147758. [CrossRef] [PubMed]
16. Yang, Z.; Yu, X.; Dedman, S.; Rosso, M.; Zhu, J.; Yang, J.; Xia, Y.; Tian, Y.; Zhang, G.; Wang, J. UAV remote sensing applications in marine monitoring: Knowledge visualization and review. *Sci. Total Environ.* **2022**, *838*, 155939. [CrossRef] [PubMed]
17. Bai, Q.-S.; Tu, S.-H. Failure analysis of a large span longwall drift under water-rich roofs and its control techniques. *Eng. Fail. Anal.* **2016**, *67*, 15–32. [CrossRef]
18. Zhao, S.; Wang, Q.; Li, Y.; Liu, S.; Wang, Z.; Zhu, L.; Wang, Z. An overview of satellite remote sensing technology used in China's environmental protection. *Earth Sci. Inform.* **2017**, *10*, 137–148. [CrossRef]
19. Hou, Y.; Zhang, A.; Lv, R.; Zhao, S.; Ma, J.; Zhang, H.; Li, Z.J.E.S.; Research, P. A study on water quality parameters estimation for urban rivers based on ground hyperspectral remote sensing technology. *Environ. Sci. Pollut. Res.* **2022**, *29*, 63640–63654. [CrossRef]
20. Carbajal-Hernández, J.J.; Sánchez-Fernández, L.P.; Villa-Vargas, L.A.; Carrasco-Ochoa, J.A.; Martínez-Trinidad, J.F. Water quality assessment in shrimp culture using an analytical hierarchical process. *Ecol. Indic.* **2013**, *29*, 148–158. [CrossRef]
21. Vahtmäe, E.; Kutser, T.; Martin, G.; Kotta, J. Feasibility of hyperspectral remote sensing for mapping benthic macroalgal cover in turbid coastal waters—A Baltic Sea case study. *Remote Sens. Environ.* **2006**, *101*, 342–351. [CrossRef]

22. Hunter, P.D.; Tyler, A.N.; Carvalho, L.; Codd, G.A.; Maberly, S.C. Hyperspectral remote sensing of cyanobacterial pigments as indicators for cell populations and toxins in eutrophic lakes. *Remote Sens. Environ.* **2010**, *114*, 2705–2718. [CrossRef]
23. Song, K.; Li, L.; Tedesco, L.P.; Li, S.; Clercin, N.A.; Hall, B.E.; Li, Z.; Shi, K. Hyperspectral determination of eutrophication for a water supply source via genetic algorithm–partial least squares (GA–PLS) modeling. *Sci. Total Environ.* **2012**, *426*, 220–232. [CrossRef] [PubMed]
24. Niu, C.; Tan, K.; Jia, X.; Wang, X. Deep learning based regression for optically inactive inland water quality parameter estimation using airborne hyperspectral imagery. *Environ. Pollut.* **2021**, *286*, 117534. [CrossRef] [PubMed]
25. Zhang, L.; Xiong, L.; Li, J.; Huang, X. Long-term changes of nutrients and biocenoses indicating the anthropogenic influences on ecosystem in Jiaozhou Bay and Daya Bay, China. *Mar. Pollut. Bulletin.* **2021**, *168*, 112406. [CrossRef] [PubMed]
26. Cong, J.-y.; Long, H.-y.; Zhang, Y.; Wang, N.J.C.G. Ecological environment response of benthic foraminifera to heavy metals and human engineering: A case study from Jiaozhou Bay, China. *China Geol.* **2022**, *5*, 12–25. [CrossRef]
27. Yu, Z.; Huang, Q.; Peng, X.; Liu, H.; Ai, Q.; Zhou, B.; Yuan, X.; Fang, M.; Wang, B. Comparative Study on Recognition Models of Black-Odorous Water in Hangzhou Based on GF-2 Satellite Data. *Sensors* **2022**, *22*, 4593. [CrossRef]
28. Greenlee, L.F.; Lawler, D.F.; Freeman, B.D.; Marrot, B.; Moulin, P. Reverse osmosis desalination: Water sources, technology, and today's challenges. *Water Res.* **2009**, *43*, 2317–2348. [CrossRef]
29. Shi, J.; Shen, Q.; Yao, Y.; Li, J.; Chen, F.; Wang, R.; Xu, W.; Gao, Z.; Wang, L.; Zhou, Y. Estimation of chlorophyll-a concentrations in small water bodies: Comparison of fused Gaofen-6 and Sentinel-2 sensors. *Remote Sens.* **2022**, *14*, 229. [CrossRef]
30. Gai, Y.; Yu, D.; Zhou, Y.; Yang, L.; Chen, C.; Chen, J. An improved model for chlorophyll-a concentration retrieval in coastal waters based on UAV-Borne hyperspectral imagery: A case study in Qingdao, China. *Water* **2020**, *12*, 2769. [CrossRef]
31. Tang, J.-W.; Wang, X.-M.; Song, Q.-J.; Li, T.; Huang, H.; Ren, J.; Jian, W. Statistical inversion models for case II water color elements in the Yellow Sea and East China Sea. *Adv. Mar. Sci.* **2004**, *22*, 1–7. [CrossRef]